J Mater Sci (2011) 46:7482–7488
DOI 10.1007/s10853-011-5718-y

Low-cost quasi-solid-state dye-sensitized solar cells based on a metal-free organic dye and a carbon aerogel counter electrode

Zhuo Tan · Bin Zhao · Ping Shen · Shenghui Jiang · Peng Jiang · Xianyou Wang · Songting Tan

Received: 10 May 2011 / Accepted: 13 June 2011 / Published online: 22 June 2011

Abstract Low-cost quasi-solid-state dye-sensitized solar cells (DSSCs) are designed and fabricated by using a metal-free organic dye and a mesoporous carbon aerogel instead of expensive ruthenium-based sensitizers and Pt electrode. The electrospun TiO_2 nanorods are added into a polyvinylidene fluoride (PVDF) solution to form a 3D network nanocomposite gel electrolyte. The presence of TiO_2 nanorods in the gel electrolyte obviously increases the ionic conductivity and decreases charge-transfer resistance of the DSSC. The effects of the gel electrolyte and the carbon aerogel counter electrode on electrochemical and photovoltaic properties have been investigated in detail. Particularly, an optimized DSSC with a nanocomposite gel electrolyte and a carbon aerogel counter electrode affords a power conversion efficiency (PCE) of 6.20% at a light intensity of 100 mW cm^{-2}.

Abbreviations

L	Liquid electrolyte
M	Normal gel electrolyte
N	Nanocomposite gel electrolyte
Cell A	Normal gel electrolyte M and Pt electrode
Cell B	Nanocomposite gel electrolyte N and Pt electrode
Cell C	Nanocomposite gel electrolyte N and carbon aerogel electrode
Cell D	Liquid electrolyte L and Pt electrode
Cell E	Normal gel electrolyte M and carbon aerogel electrode

Z. Tan · B. Zhao · P. Shen · S. Jiang · P. Jiang · X. Wang · S. Tan (✉)
College of Chemistry, Key Laboratory of Environmentally Friendly Chemistry and Applications of Ministry of Education, Xiangtan University, Xiangtan 411105, People's Republic of China
e-mail: tanst2008@163.com

B. Zhao · P. Shen · S. Tan
Key Laboratory of Advanced Functional Polymeric Materials of College of Hunan Province, Xiangtan University, Xiangtan 411105, People's Republic of China

Introduction

Since the discovery of nanocrystalline dye-sensitized solar cells (DSSCs) in 1991 [1], the highest power conversion efficiency (PCE) of over 11% has been achieved by the use of organic dyes and liquid electrolytes [2, 3]. The relatively high performance and low production cost render DSSCs as competitive alternatives to conventional silicon-based photovoltaic devices [4]. However, several technological challenges have to be overcome until DSSCs can be produced on a large scale. On the one hand, the presence of liquid electrolytes may result in some practical limitations of sealing and long-term stability. On the other hand, ruthenium-based sensitizers and Pt counter electrode are too expensive and unrenewable for practical application.

Further enhancement in PCE and decrease in the production cost are highly desired for commercialization of DSSCs. Recently, DSSCs employing quasi-solid polymer electrolytes have been investigated intensively because of their intrinsic advantages, such as a low evaporation and a long-term stability [5–8]. Consequently, many efforts have been devoted to prepare quasi-solid polymer electrolytes by the use of polymers [9, 10], inorganic nanofillers [11, 12], and small molecule plasticizers [13]. However, the DSSCs based on polymer electrolytes often exhibit a lower overall conversion efficiency than those based on liquid electrolytes, mainly due to the inferior mass-transfer rates of the redox couples (I^-/I_3^-) in the highly viscous

media and the decreased electron-transfer at the electrolyte/electrode interfaces [14]. Therefore, it is very important to improve the photovoltaic performances by increasing the ion mobility of quasi-solid polymer electrolyte.

Moreover, photosensitizers play a crucial role in the construction of highly efficient DSSCs. Although a DSSC based on the ruthenium complex, N719 dye [15], shows the highest PCE in standard air mass 1.5 sunlight, DSSCs based on metal-free organic dyes hold the promise by virtue of low-cost, high molar extinction coefficients, and easily modified molecular structures. Our group has reported a series of metal-free triphenylamine-based organic dyes for DSSCs [16, 17]. It turns out that they reveal a relatively high photovoltaic performance, comparable to those of ruthenium-based systems.

With respect to the counter electrode, as a key component of DSSC, a thin layer of Pt catalyst deposited on transparent conductive oxide substrates is widely employed [18–20]. But it is noticeable that Pt is expensive and there are also some reports of corrosion of Pt in triiodide-containing solutions [21, 22]. Much attention has been paid to porous carbon materials as potential alternatives in recent years. Unfortunately, it appears that the carbon material electrodes have a much higher electrical resistance than the Pt electrode and maybe lower catalytic activity [23], leading to the low PCE. As a consequence, it is highly desirable to develop a cost-effective electrocatalyst for practical application of DSSCs.

In this present work, the aforementioned key components of DSSCs have been taken into account to develop a new type of quasi-solid-state dye-sensitized solar cells. At first, we prepared a nanocomposite gel electrolyte by dispersing TiO_2 nanorods into quasi-solid PVDF-based gel electrolyte. The photovoltaic performances of the corresponding quasi-solid-state DSSCs were enhanced by introducing TiO_2 nanorods. To lower the production costs, the metal-free organic dye H1 (shown in Fig. 1) with a high power conversion efficiency of 9.1% in liquid state electrolyte [24] was chosen as the substitute for expensive Ru-based dyes. At last, a type of carbon aerogel coated on the stainless steel mesh was explored as a counter electrode to replace the expensive Pt electrode as it is easily prepared and low-cost. The morphology and photovoltaic properties of the novel quasi-solid-state DSSCs have been investigated in detail.

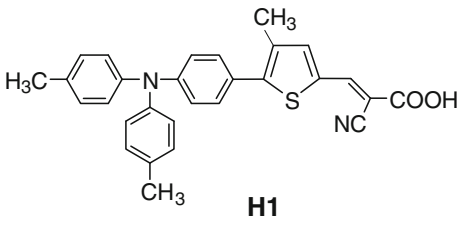

Fig. 1 Molecular structures of the dye H1

Experimental section

Materials

All the reagents used were of analytical grade. TiO_2 powder (P25, Degussa AG, Germany) consists of 30 wt% rutile and 70 wt% anatase. Conductive glass of fluorine-doped SnO_2 (FTO, 14 Ω sq^{-1}) was purchased from NSG Co. of Japan. The metal-free organic dye H1 and TiO_2 nanorods were synthesized and prepared according to the literature procedures [24, 25].

Preparation of the electrolytes and the carbon aerogel electrode

Liquid electrolyte (L) consists of 0.6 M 1-methyl-hexylimidazolium iodide (MHII), 0.5 M LiI, 0.05 M I_2, and 0.5 M 4-*tert*-butylpyridine (TBP) in 3-methoxypropionitrile. The normal gel electrolyte (M) was prepared by adding 10 wt% PVDF (based on L) into the electrolyte L. The nanocomposite gel electrolyte (N) was prepared by adding 5 wt% TiO_2 nanorods as nanofiller into the electrolyte M, whereby the TiO_2 nanorods were fabricated by combining sol–gel and electrospinning techniques [25]. All mixtures (electrolytes M and N) were sonicated 30 min and then heated with vigorous stirring for 2 h. After cooling down to room temperature, the normal gel electrolyte M and the nanocomposite gel electrolyte N were formed. Stainless steel mesh (the thickness of the mesh is 140 μm, the aperture is 94 μm) was ultrasonically cleaned in isopropanol for 15 min, rinsed with ethanol, and finally dried prior to use. Carbon aerogel was mixed with 60%-water PTFE suspension (quality ratio of carbon aerogel to PTFE is 9:1), followed by adding ethanol and ultrasonically dispersing for 15 min. The resulting homogeneous mixture was spreaded on stainless steel mesh, and dried in vacuum at 50 °C for 48 h. Finally, the dried electrode was compressed under pressure about 20 MPa to produce a 50 μm thick film. Fluorine-doped SnO_2 conducting glass (FTO) was cleaned and immersed in aqueous 40 mM $TiCl_4$ solution at 70 °C for 30 min, then washed with water and ethanol, sintered at 450 °C for 30 min. The 20–30 nm particle-sized TiO_2 colloid blended with 0.1 wt% magnesium acetate solution was coated onto the FTO glass by sliding glass rod method to obtain a TiO_2 film of 10–15 μm thickness after drying. The 200 nm particle-sized TiO_2 colloid was coated on the electrode by the same method, resulting in a TiO_2 light-scattering layer of 4–6 μm thickness. The TiO_2 electrodes were immersed in a solution of

H1 dye (0.5 mM) in acetonitrile at room temperature. After dye adsorption, the dye-coated TiO_2 electrodes were copiously rinsed with ethanol. The photovoltaic measurements were performed in a sandwich cell consisting of the H1 dye-sensitized TiO_2 electrode as the working electrode and Pt foil or carbon aerogel as the counter electrode.

Measurement and characterization

The morphology and microstructrues of the prepared nanorods were analyzed by field emission-scanning electron microscope (SEM) (Leo-1525, Carl Zeiss, Germany). The photocurrent–voltage curves of solar cells were measured using a Keithley 2602 Source meter under the 100 mW cm^{-2} irradiation of a CHF-XM 500 W Xe lamp with a global AM 1.5 filter for solar spectrum simulation, and the efficient irradiated area of cell was 0.196 cm^2. The light intensity of the illumination source was calibrated by using a standard silicon solar cell. Furthermore, the incident photon-to-current conversion efficiency (IPCE) was measured by using a Zolix DCS300PA199 Data acquisition system. The ionic conductivity was measured by cyclic voltammetry with a sandwich cell composed of two mirror-finished Pt foil electrodes separated by a 50 μm spacer, the scan rate was 5 mV and the measurement was carried out at 25 °C on an IM6e potentiostat (Zahner, Germany). Impedance measurements were also performed with IM6e potentiostat in the frequency range of 0.1 Hz–1000 kHz under dark conditions. The AC amplitude and the applied voltage of the cells were 5 mV and −0.68 V, respectively. The impedance spectra were fitted with Z-View software in terms of appropriate equivalent circuits.

Results and discussion

Morphology and structure characterization

SEM image of the electrospun TiO_2 nanorods is shown in Fig. 2a. The nanorods with a diameter of 50–200 nm and a length of 1–10 μm link each other in the polymer PVDF/3-methoxypropionitrile solution, forming a 3D network quasi gel electrolyte. As shown in Fig. 2b, both the uniform motionless electrolyte M (left, dark reddish brown) and nanocomposite gel electrolyte N (right, yellow) were obtained after cooling down to room temperature. The liquid solvent filled the space of the network. In addition, the TiO_2 nanorods in the polymer medium lead to a light-scattering effect [15], which can increase effectively the light-harvesting efficiency.

Table 1 summarizes the photovoltaic performances of DSSCs based on different types of electrolytes and counter electrodes under irradiation of AM 1.5 (100 mWcm^{-2}). The *J–V* curves of the DSSCs with quasi-solid electrolytes are shown in Fig. 3. The cell A with the gel electrolyte M and Pt electrode exhibits a PCE of 5.76%, which is 2/3 lower than that of cell D (9.10%, Table 1) with the liquid electrolyte and Pt electrode. Compared with the cell A, the cell B with the nanocomposite gel electrolyte N and Pt electrode reveals a markedly improved PCE (6.71%), indicating that the addition of the TiO_2 nanorods into the gel electrolyte M gives rise to a remarkable increase in the short circuit current (J_{SC}) without a significant change of the open circuit voltage (V_{OC}). It is possible and reasonable considering that the nanocomposite electrolyte has a higher ion diffusion coefficient, but a lower internal resistance than the gel electrolyte M, as discussed in the following part.

Photovoltaic performances of DSSCs

As illustrated in Fig. 3, the V_{OC} value of the cell C using the carbon aerogel counter electrode increases by 60 mV than that of the cell B using the Pt electrode with the same electrolyte N. However, the cell C shows a slightly lower PCE (6.20%) than that of the cell B because of the considerably lower J_{SC}. This observation can be accounted for the fact that the redox potential of I_3^-/I^- positively shifts because of a large charge-transfer resistance R_{CT} for the I_3^-/I^- redox reaction in the case of the carbon aerogel counter electrode [23, 26].

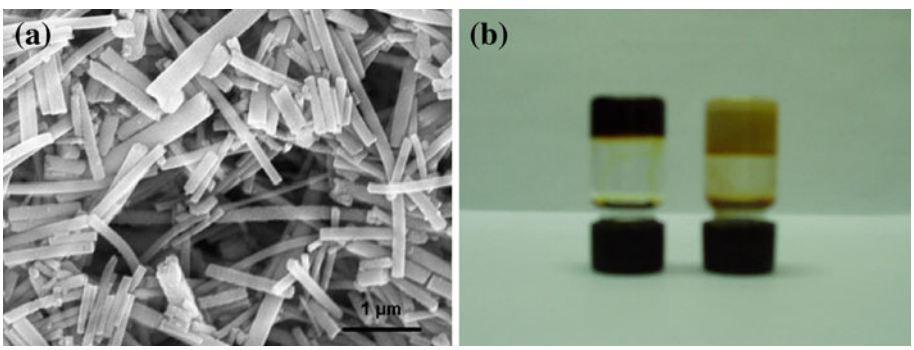

Fig. 2 (**a**) SEM images of electrospun TiO_2 nanorods and (**b**) the photo of the normal gel electrolyte M (*left*) and the nanocomposite gel electrolyte N (*right*)

Table 1 Photovoltaic properties of different dye-sensitized solar cells

Cells	J_{sc} (mA/cm^{-2})	V_{oc} (V)	FF	η (%)
Cell A	12.14	0.68	0.70	5.76
Cell B	15.69	0.67	0.64	6.71
Cell C	11.89	0.73	0.71	6.20
Cell D	18.03	0.72	0.70	9.10
Cell E	10.46	0.72	0.73	5.49

Note: cells A, B, and C are the same as those in Fig. 3, *cell D* liquid electrolyte L and Pt electrode, *cell E* normal gel electrolyte M and carbon aerogel electrode

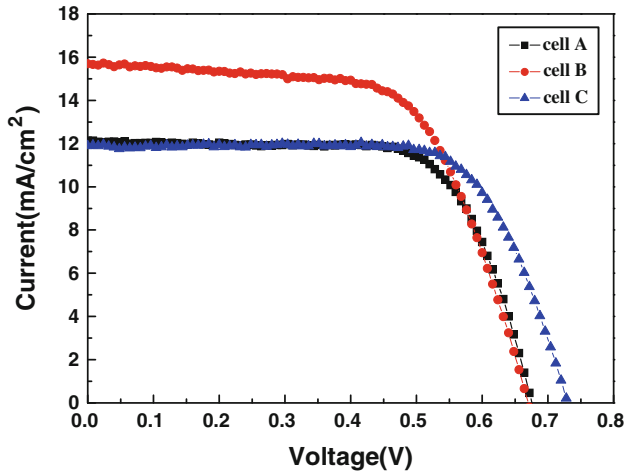

Fig. 3 *J–V* curves of DSSCs cell: *cell A* normal quasi-solid electrolyte and Pt electrode; *cell B* nanocomposite gel electrolyte and Pt electrode; *cell C* nanocomposite gel electrolyte and carbon aerogel electrode

Figure 4 presents the incident photon-to-current conversion efficiency (IPCE) curves of three photovoltaic cells, showing that the higher IPCE value gives a higher J_{SC}. Notably, the cell B has IPCE values of >70% between 400 and 500 nm. The enhanced cell performance of the cell B may be because of the improved ion conductivity and light-scattering effect of the nanorods. Despite of the low J_{SC}, the cell C exhibits a PCE quite similar to that of the cell B due to its high V_{OC}. Moreover, the cells A and C possess similar IPCE values leading to the similar J_{SC}, and a higher PCE of the cell C (6.20%) than that of cell A (5.76%) is attributed to the high V_{OC} of the former.

Ion transport performance in electrolytes

Diffusion-limited currents within the electrochemical cell were determined by cyclic voltammetry measurements at a scan rate of 5 mVs^{-1}. Figure 5 shows the

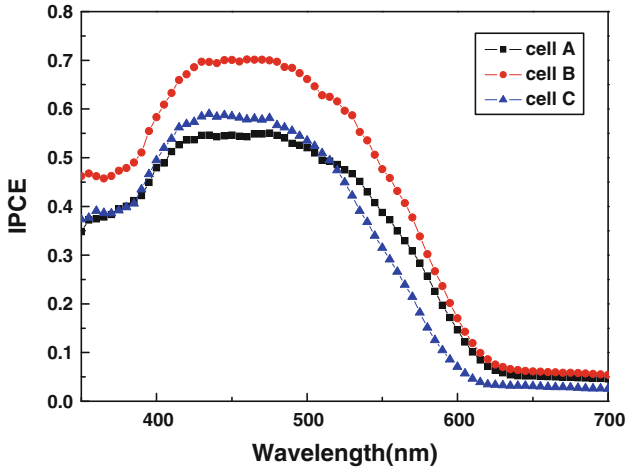

Fig. 4 IPCE plots for the DSSCs A–C

diffusion-limiting currents in the different electrolytes at 25 °C. The current is mainly limited by the diffusion of I_3^- because of the large excess of I^- in the electrolyte [27, 28]. In the cell by means of the expression [29]:

$$D_{I_3^-} = \frac{1}{2nFc_{I_3^-}} J_{\lim}$$

where $n = 2$ is the number of electrons involved in the electrochemical reduction of triiodide at the electrode, F is Faraday's constant, $c_{I_3^-}$ is the concentration per volume unit of I_3^-, assumed uniform along the whole cell, and l is the distance between the electrodes, $J_{\lim}$ is saturation of the current density. When the PVDF added to a liquid electrolyte L, the $D_{I_3^-}$ values decreased from 4.0×10^{-6} to 1.2×10^{-6} cm^2 s^{-1} due to the increased macroscopic viscosity of the gel electrolyte M. In comparison with the gel electrolyte M, the nanocomposite gel electrolyte N shows a higher $J_{\lim}$ value and the corresponding $D_{I_3^-}$ is 2.6×10^{-6} cm^2 s^{-1} at 25 °C, which is also lower than that of the liquid electrolyte L. These results indicate that the 3D network of the nanocomposite gel electrolyte N forms an effective pathway for the transport of redox species, whereby these charges could be transported freely in the channels of the nanocomposite gel network. This special charge transport mechanism, interpreted as an increased charge exchange mechanism, i.e. Grotthuss mechanism [13], is contributed to the effective charge transport properties of an I_3^-/I^- redox couple in the nanocomposite gel electrolyte as demonstrated in the literature [8, 30].

Impedance of DSSCs

Electrochemical impedance spectroscopy (EIS) was performed to analyze internal resistance in DSSCs, Fig. 6

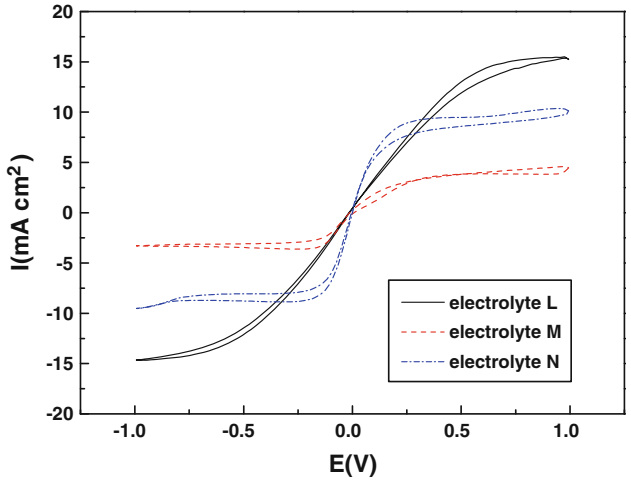

Fig. 5 Diffusion-limiting currents in the different electrolytes at 25 °C

depicts the fitted Nyquist plots (Fig. 6a) and Bode phase angles (Fig. 6b) of the DSSC experiments carried out under dark conditions at −0.68 V bias. The charge-transfer resistances at the counter electrode/electrolyte interface (R1) and at the dyed TiO_2/electrolyte interface (R2) correspond to the semicircles in the frequency regions 10^3–10^5 Hz and 1–10^3 Hz [31], respectively. Pt/electrolyte interface in cells A and B shows similar $R1$ values (2.70 and 3.05 Ω cm^2 in Table 2), whereas the carbon aerogel electrode/electrolyte interface in the cell C has the $R1$ value of 4.42 Ω cm^2. Smaller $R1$ value of the Pt/electrolyte interface suggests a higher electorcatalytic activity than that of carbon aerogel/electrolyte interface. At high frequency region (10^3–10^6 H_Z), the impedance is dominated by the RC network of the electrode/electrolyte interface, consisting of the R_{ct} and the capacitance of electrical double layer (i.e., CDL) [32]. At a given potential, it is obvious that the value of $R2$ decreases from 47.94 to 27.45 Ω cm^2 (Table 2) when adding TiO_2 nanorods into the normal gel electrolyte M, indicating that electron transport increases at the dyed TiO_2/electrolyte interface. Both the charge transport in the nanocomposit gel electrolyte N and the transportation of I_3^- ions from the dyed

Table 2 Parameters obtained by fitting the impedance spectra of cells shown in Fig. 6a

Cells	R_S (Ω cm^2)	R_1 (Ω cm^2)	C_1 (F cm^{-2})	R_2 (Ω cm^2)	C_2 (F cm^{-2})
Cell A	23.76	2.70	1.24E−5	47.49	8.34E−4
Cell B	22.36	3.05	1.77E−5	27.45	6.50E−4
Cell C	20.30	4.42	7.83E−6	91.41	3.59E−4

TiO_2/electrolyte interface to the counter electrode are faster than those in the normal gel electrolyte M, resulting in a higher photocurrent and IPCE value of the cell B with the nanocomposite gel electrolyte. Furthermore, the significantly large $R2$ values in both cells A and C imply the retardation of the charge recombination between injected electron and electron acceptor I_3^- in the electrolyte, leading to an increase in V_{OC} [33]. These results are not only consistent with the above-mentioned trend in the change of V_{OC} values in cells A–C, but also with the measured dark current (Fig. 7).

Photostability of DSSCs

Since the nanocomposite quasi-solid-state solar cell C assembled with H1 metal-free organic dye and a carbon gel counter electrode shows a good photovoltaic performance, we further tested its long-term photostability. Figure 8 exhibits the normalized efficiency variation of the cell C with time during successive light soaking (100 mW cm^{-2}). After successive light irradiated at room temperature for 1 month (about 700 h), the cell C maintains 90% of its initial power conversion efficiency, indicative of a good photostability. Thus, our approach paves the way to design steady efficiency and low-cost DSSCs.

Conclusions

In summary, we prepared a new type of dye-sensitized solar cells with the nanocomposite gel electrolyte and a

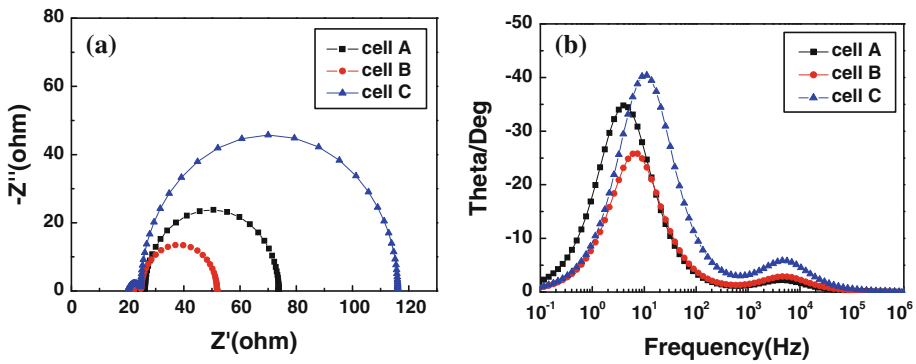

Fig. 6 Nquist plots (**a**) and Bode plots (**b**) of different cells measured at −0.68 V

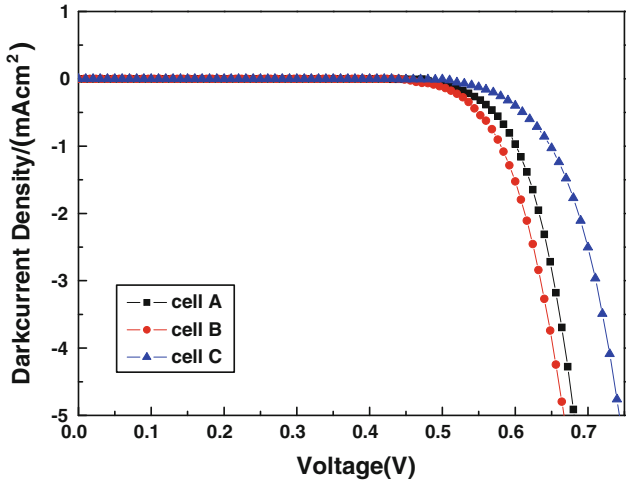

Fig. 7 Dark current–voltage characteristics of different cells

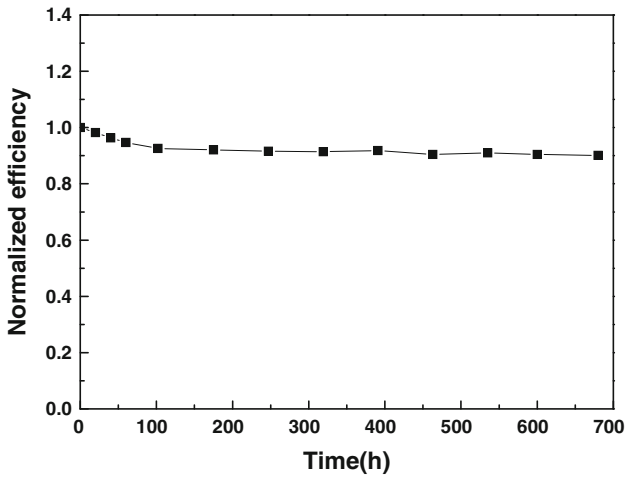

Fig. 8 Normalized efficiency variation of the cell C with time during successive light soaking (100 mW cm^{-2})

carbon areogel counter electrode. The TiO_2 nanorods were added into the PVDF gel electrolyte forming a 3D network gel electrolyte in order to facilitate the ion transport in a highly viscous medium. The nanocomposite gel electrolyte N exhibits considerable ionic conductivity and a triiodide ionic diffusion constant. Therefore, DSSCs (B and C) based on the gel electrolyte N exhibit much better photovoltaic performance and photostability than the cell A with the normal gel electrolyte. Furthermore, the introduction of metal-free organic dye and a carbon areogel counter electrode offers a new perspective in the application of low-cost DSSCs. The optimization of these parameters allows us to attain the cell C with good photovoltaic performances. Further investigations to achieve even more cost-effective and long-term stable DSSCs are in progress.

Acknowledgements This work was supported by the National Natural Science Foundation of China (Nos. 50973092, 51003089) and Open Fund of Key Laboratory of Advanced Functional Polymeric Materials of College of Hunan Province (Nos. 09K037).

References

1. O'Regan B, Grätzel M (1991) Nature 353:737
2. Nazeeruddin MK, Angelis FD, Fantacci S, Selloni A, Guido V, Liska P, Ito S, Takeru B, Grätzel M (2005) J Am Chem Soc 127:16835
3. Chiba Y, Islam A, Watanabe Y, Komiya R, Koide N, Han L (2006) Jpn J Appl Phys 45:638
4. Gonçalves LM, Bermudez VZ, Ribeiro HA, Mendes AM (2008) Energy Environ Sci 1:655
5. Stergiopoulos T, Arabatzis IM, Katsaros G, Falaras P (2002) Nano Lett 2:1259
6. Wang P, Zakeeruddin SM, Exnar I, Grätzel M (2002) Chem Commun 2972
7. Stathatos E, Lianos P, Lavrencic-Stangar U, Orel B (2002) Adv Mater 14:354
8. Huo Z, Dai S, Wang K, Kong F, Zhang C, Pan X, Fang X (2007) Sol Energy Mater Sol Cells 91:1959
9. Xia JB, Li FY, Yang H, Li XH, Huang CH (2007) J Mater Sci 42:6412. doi:10.1007/s10853-010-4925
10. Wang M, Pan X, Fang X, Guo L, Liu W, Zhang C, Huang Y, Hu L, Dai S (2010) Adv Mater 22:5526
11. Wang P, Zakeeruddin SM, Comte P, Exnar I, Grätzel M (2003) J Am Chem Soc 125:1166
12. Lin C, Tu W, Kuo C, Chien S (2011) J Power Sources 196:4865
13. Kubo W, Murakoshi K, Kitamura T, Yoshida S, Haruki M, Hanabusa K, Shirai H, Wada Y, Yanagida S (2001) J Phys Chem B 105:12809
14. Kang M, Ahn K, Lee J (2008) J Power Sources 180:896
15. Nazeeruddin MK, Kay A, Rodicio L, Humphry-Baker R, Müller E, Liska P, Vlachopoulos N, Grätzel M (1993) J Am Chem Soc 115:6382
16. Shen P, Liu Y, Huang X, Zhao B, Xiang N, Fei J, Liu L, Wang X, Tan S (2009) Dyes Pigments 83:187
17. Chen H, Huang H, Huang X, Clifford JN, Forneli A, Palomares E, Zheng X, Zheng L, Wang X, Shen P, Zhao B, Tan S (2010) J Phys Chem C 114:3280
18. Papageorgiou N, Maier WF, Grätzel M (1997) J Electrochem Soc 144:876
19. Fang X, Ma T, Guan G, Akiyama M, Kida T, Abe E (2004) J Electroanal Chem 570:257
20. Kim S, Nah Y, Noh Y, Jo J, Kim D (2006) Electrochim Acta 51:3814
21. Kay A, Grätzel M (1996) Sol Energy Mater Sol Cells 44:99
22. Olsen E, Hagen G, Lindquist SE (2000) Sol Energy Mater Sol Cells 63:267
23. Imoto K, Takatashi K, Yamaguchi T, Komura T, Nakamura J, Murata K (2003) Sol Energy Mater Sol Cells 79:459
24. Jiang S, Zhou W, Tan Z, Shen P, Zhao B, Tan S (2011) Scientia Sinica Chimica 41:982
25. Huang X, Shen P, Zhao B, Feng X, Jiang S, Chen H, Li H, Tan S (2010) Sol Energy Mater Sol Cells 94:1005
26. Fang B, Fan S, Kim J, Kim M, Kim M, Chaudhari NK, Ko J, Yu J (2010) Langmuir 26:11238
27. Shi J, Peng S, Pei J, Liang Y, Cheng F, Chen J (2009) Appl Mater Interfaces 1:944
28. Hauch A, Georg A (2001) Electrochim Acta 46:3457
29. Fabregat-Santiago F, Bisquert J, Palomares E, Otero L, Kuang D, Zakeeruddin SM, Grätzel M (2007) J Phys Chem C 111:6550

30. Kang S, Kim J, Kim H, Koh H, Lee J, Sung Y (2008) J Photochem Photobiol A Chem 200:294
31. Xia J, Masaki N, Lira-Cantu M, Kim Y, Jiang K, Yanagida S (2008) J Am Chem Soc 130:1258
32. Wang G, Xing W, Zhuo S (2009) J Power Sources 194:568
33. Shen P, Tang Y, Jiang S, Chen H, Zheng X, Wang X, Zhao B, Tan S (2011) Org Electron 12:125